Ultrasensitive In Situ Fluorescence Analysis using Modulated Fluorescence Interference Contrast at Nanostructured Polymer Surfaces

Xiaopei Deng, Siheng He, Fan Xie, Christian Friedmann, Henry Hess, and Joerg Lahann**

Fluorescence-based imaging is widely used in biotechnology, environmental detection, and medical diagnostics, because it can resolve objects at the nanometer to micrometer scale.[1] Main drawbacks of fluorescence measurements include insufficient brightness of the fluorophores, high background fluorescence, and, as a result, inadequate signal-to-noise ratios. Although major efforts have been directed toward improved fluorescence probes with higher brightness and better photostability,[2–6] current progress is hampered by increasingly complicated (and expensive) syntheses of the fluorescent probes with often still insufficient quantum yields.[4,7] Several alternative strategies have been pursued including metal-enhanced fluorescence,[8–11] or photonic crystal enhanced fluorescence.[12]

In addition to limitations associated with inadequate fluorophores, a spectrum of experimental factors can contribute to increased noise, including excess background fluorescence from out-of-focus planes,[13] lens effects,[14] or inhomogeneous illumination.[15] To better account for experimental influences, the background signal can be subtracted from the actual fluorescence signal by comparing binding regions and nonbinding reference regions within the same field of view using substrates with microstructured thickness differences.[16,17]

In this study, we introduce a novel type of fluorescence analysis substrates that uses precisely engineered polymer nanofilms of appropriate thickness to simultaneously: i) amplify the fluorescence signal of the test regions and ii) extinguish the fluorescence of the reference regions (**Figure 1**). A main advantage of this approach is that the chemical nature of the polymer substrate is identical throughout the entire system, thereby eliminating the need to create a specialized surface chemistry in the reference region, which suppresses the binding of the fluorescent species. This advantage can be further amplified by an extension of the classic lock-in detection concept[18] toward the analysis of patterned surfaces to eliminate background-related noise.

In principle, the amplification and elimination of the fluorescence signal on nanofilms with defined topology relies on the exploitation of fluorescence interference contrast above a reflective surface.[19–21] Interference between the direct and reflected excitation light, as well as interference between the direct and reflected fluorescence emission, can cause extinction of the fluorescence signal at the surface and at half of a wavelength of optical path length (nanofilm refractive index of 1.64) above the surface, and maximization of the fluorescence signal at one fourth and three fourth of a wavelength above the surface (Figure 1c; see Supporting Information for details about the theoretical predictions). The modulation of the fluorescence signal becomes less pronounced at larger distances due to the large aperture of the objective and the unequal excitation and emission wavelengths.[22] In addition to the modulation of the fluorescence signal, which is also observed on nonmetallic reflecting substrates such as silicon, the nanoscale structure of the deposited gold film causes a strong amplification of the signal referred to as metal-enhanced fluorescence (MEF).[23–25] Transparent spacer layers, such as silica,[24,26,27] with precisely controlled thickness have been employed to achieve a maximum enhancement of the fluorescence signal. By creating imaging substrates with areas of thicknesses that extinguish the fluorescence signal (reference area) and areas that amplify the signal (test area), highly sensitive measurements can be conducted.

Here, these effects are illustrated using fluorescein-labeled bovine serum albumin (FITC-BSA) as a model protein that binds to the polymer surface via nonspecific adsorption (Figure 1). In this experiment, the dielectric spacer layer is realized by depositing a polymer layer of poly(4-chloro-*p*-xylylene) on gold-coated glass using chemical vapor deposition (CVD) polymerization.[28] The CVD process ensures nanometer control and excellent reproducibility of the spacer thickness[29] (Note 1, Supporting Information). Based on experimental measurement and theoretical considerations (Figure 1c), a layer thickness of 43 nm was selected to yield the maximal signal (test area) and a layer thickness of 120 nm was selected to null the fluorescence signal (reference area) from the adsorbed FITC-BSA. Importantly, X-ray photoelectron spectroscopy (XPS) elemental analysis confirms the chemical identity of the test and reference regions (Figure 1b and Note 2, Supporting Information), which unambiguously confirms that the surface is chemically uniform throughout the test region and independent of the film thickness.

Because the fluorescence signal from the surface of the reference region must be zero, the detected reference signal can be attributed

Dr. X. Deng, F. Xie, Prof. J. Lahann
Biointerfaces Institute & Chemical Engineering
University of Michigan
Ann Arbor, MI 48109, USA
E-mail: lahann@umich.edu
S. He, Prof. H. Hess
Biomedical Engineering
Columbia University
New York, NY 10027, USA
E-mail: hhess@columbia.edu
C. Friedmann, Prof. J. Lahann
Institute of Functional Interfaces
Karlsruhe Institute of Technology
Hermann-von-Helmholtz-Platz 1
76344 Eggenstein-Leopoldshafen, Germany

DOI: 10.1002/adma.201505197

ADVANCED MATERIALS
www.advmat.de

www.MaterialsViews.com

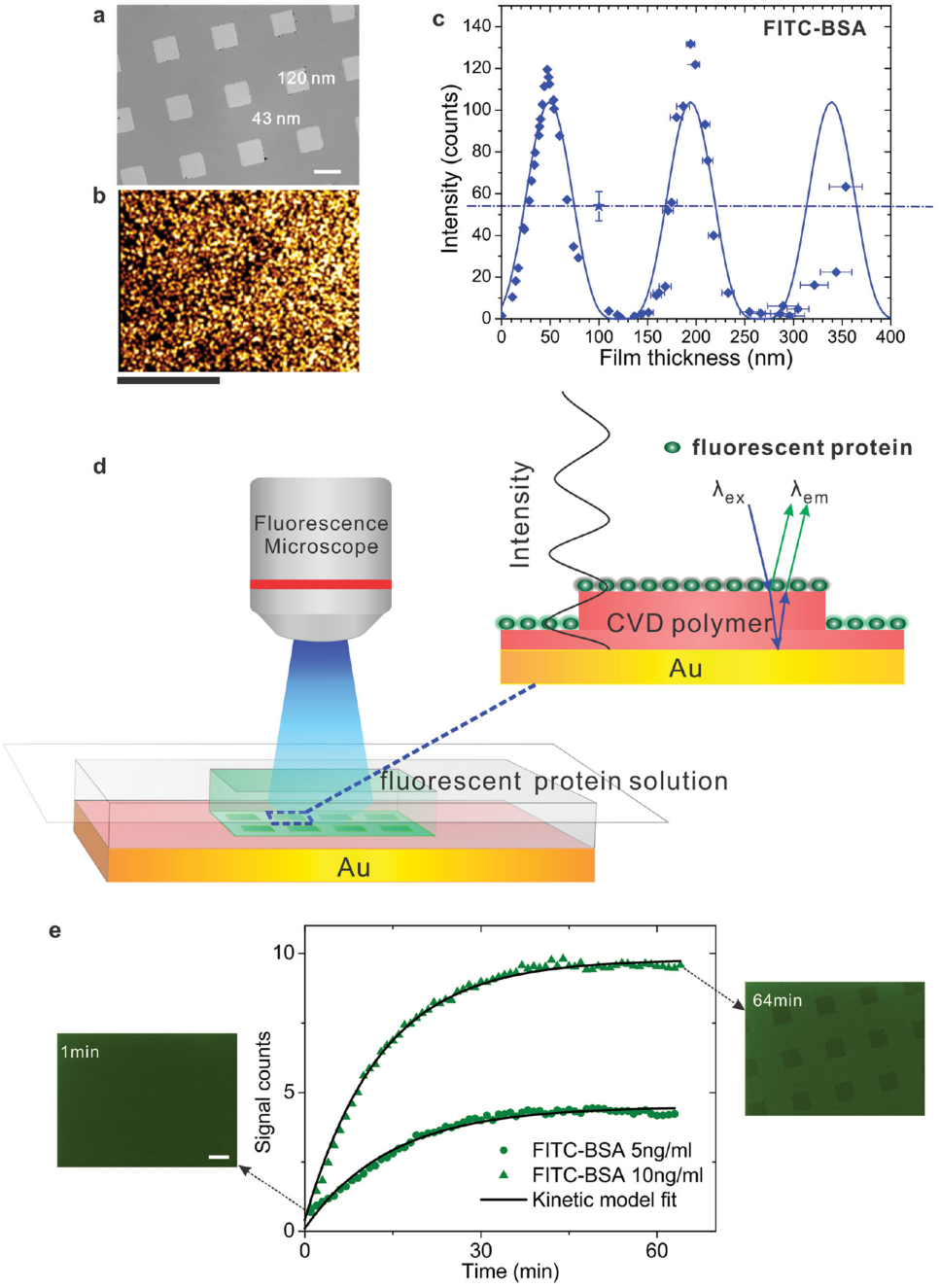

Figure 1. Real-time monitoring of FITC-BSA adsorption on poly(4-chloro-*p*-xylylene). a) Bright-field images of the patterned surface of poly(4-chloro-*p*-xylylene) on a gold surface. The thicknesses of the nanoscale polymer layer inside the squares and outside the squares are 43 and 120 nm respectively. b) XPS imaging of Au 4f scans reveal no contrast on a patterned surface coated with a polymer film that has thicknesses of 25 nm outside the squares and 60 nm inside the squares. This confirms that the gold surface is fully covered with poly(4-chloro-*p*-xylylene) and chemically identical (More details are provided in Note 2 in the Supporting Information). c) A series of gold surfaces coated with nanoscale polymer films of different thicknesses were incubated in 0.5 mg mL^{-1} FITC-BSA for 90 min, thoroughly rinsed, air dried and imaged in the FluorChem M digital dark room with an exposure time 500 ms. Both the experimental data (the diamond dots) and the fitted curve (the solid line) are plotted. For reference, the dash-dot line presents the fluorescence intensity of the FITC-BSA adsorbed on bare glass coated with poly(4-chloro-*p*-xylylene). d) The setup for real-time monitoring of the protein adsorption under an epifluorescence microscope using a simple solution cell consisting of the fabricated pattern surface shown in (a), a piece of thin PDMS layer with a punched hole and a piece of cover glass. FITC-BSA adsorbed equally everywhere on the surface, but revealed different fluorescence intensity on and off the pattern squares due to the different interference effect from different polymer spacer layer thicknesses. e) Real-time monitoring of FITC-BSA adsorption using the nanoscale amplification substrates. The concentrations used are in the picomolar range (5 ng mL^{-1} equals 76 pM for FITC-BSA). The experimental kinetics data (the solid circles and triangles) generated by lock-in analysis of the fluorescence microscope images were taken every minute and follow a first-order rate model (solid lines). All scale bars represent 200 μm.

to the experimental background and can thus be subtracted from the test signal to remove contributions associated with the imaging environment or imaging artifacts. By direct observation of test and reference regions within the same field of view, this analysis platform can thus provide direct in situ observation of surface-binding kinetics and enables real-time monitoring of protein adsorption, antibody binding and other interfacial interactions (Figure 1e).

The fundamental challenge of signal extraction in systems with low signal-to-noise ratios is not specific to fluorescence measurements, but similarly applies to infrared spectroscopy, molecular-beam spectroscopy[30] and resistance thermometry. This challenge is frequently addressed by applying signal processing methods, such as lock-in amplification methods. The concepts underlying these signal processing algorithms can in principle be translated from time-resolved measurements to spatially resolved measurements.[31] Here, the ability provided by the CVD process to generate highly reproducible patterned surfaces with regions where the fluorescence is either maximized or absent, enables the application of the lock-in concept to the problem of recovering a fluorescence signal from the binding of molecules to a surface. Rather than using a lock-in amplifier to recover a signal, which is modulated in time, we now introduce an algorithm, which recovers a fluorescence signal from a known spatial pattern in an image (modulating the signal in two spatial dimensions). The algorithm cross-correlates the fluorescence microscopy image of the surface with the surface pattern of known thickness regions (Figure 5c), automatically aligns the image and the pattern, and extracts the portion of the fluorescence signal, whose modulation conforms to the pattern, while rejecting contributions to the fluorescence signal, which arise from high-frequency noise or slow variations in the background signal. More details regarding lock-in analysis will be discussed later.

Figure 1e summarizes experimental results, wherein the substrate shown in Figure 1a was exposed to a FITC-BSA for times ranging from 1 to 64 min under identical imaging conditions. As a result of the adsorption of FITC-BSA, a visible contrast between test and reference areas emerges over time. However, the lock-in analysis of the images is able to remove noise from background fluorescence to such a degree that the contrast between test and reference areas is already detectable at the first data point, when the fluorescence from the test area has increased by less than one count in average. As expected, the adsorption of FITC-BSA to the polymer-coated surface follows first-order kinetics. Practically important, the fluorescence signal does not decline over time indicating the absence of photobleaching over the observation period.

The particular approach used for fabrication of variable thickness spacer layers on the same gold substrate through a CVD process[32] is illustrated in **Figure 2**a. The CVD polymerization is a versatile coating technology that allows for ultraprecise thickness control, while providing a wide selection of functional groups for subsequent bioconjugation, including aldehyde, ketones, amine, alkyne, vinyl, maleimide, anhydride, active ester, hydroxyl, fluorine, or photo-reactive benzoyl groups.[33] In the examples shown in Figure 2, the particular CVD polymer carries aldehyde groups that can be used to covalently attach fluorescent molecules via

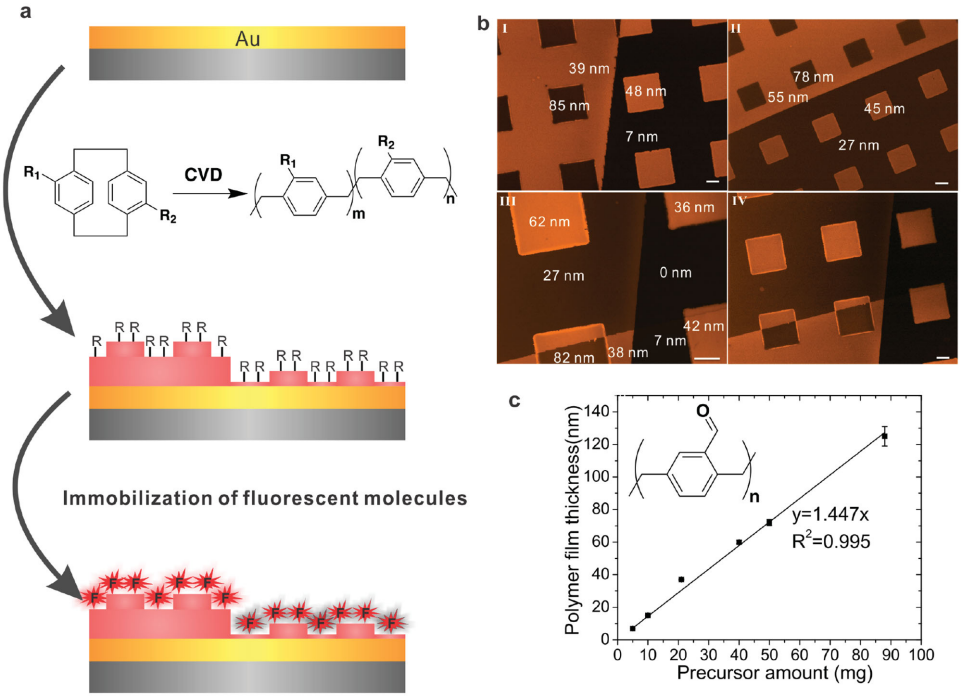

Figure 2. Preparation of nanoscale amplification substrates. a) CVD polymerization of various [2.2]paracyclophanes leads to polymer spacer layers with functional groups for further immobilization of biomolecules. Fluorescent molecules can be immobilized to the space layer via physical adsorption or covalent reaction. b) Fluorescence microscopy images of Alexa 555 hydrazide dye immobilized on patterned substrates made of polymer 1 with aldehyde functional groups. The polymer layer thicknesses of different pattern regions were measured by imaging ellipsometer and noted in the figure. We note that (III) is the high magnification image of the sample shown in (IV). Scale bars represent 100 μm. c) The film thickness of polymer 1 and the precursor amount is plotted in the graph. When other deposition parameters are fixed, the polymer film thickness can be controlled by the precursor amount following a linear relationship.

hydrazide coupling. A gold substrate featuring aldehyde-functionalized spacer layers with different thicknesses was prepared by CVD polymerization for subsequent covalent immobilization of Alexa Fluor 555 hydrazide. The high degree of linearity of the relationship between precursor amount and polymer film thickness enables control over the film thickness with nanometer precision and excellent uniformity (Figure 2c). The chemically homogenous polymer surfaces were then analyzed by fluorescence microscopy (Figure 2b). While the covalent immobilization of fluorescent dye is homogenous throughout the entire field of view, a clear contrast in the fluorescence intensity can be detected between surface regions of different polymer thicknesses.

The importance of the gold substrate is illustrated by a direct comparison with silicon as substrate material in a experiment, where gold islands were deposited onto silicon wafers and then uniformly coated with CVD polymer **1** at a constant polymer thickness. The signal-enhancing character of the gold coating compared to polished bare silicon was confirmed (**Figure 3**a). In another experiment, polymer-coated surfaces with various polymer layer thicknesses, as noted in Figure 3b–g, were incubated with Alexa Fluor 555 hydrazide (10 µg mL^{-1} in water, 12 h) (Figure 3b,c) or Alexa Fluor 488 conjugated fibrinogen (100 µg mL^{-1} in PBS, 4 h) (Figure 3d–g) and thoroughly rinsed prior to imaging. Alexa Fluor 555 hydrazide was covalently immobilized following the experimental procedure outlined in Figure 2, while fibrinogen adsorbs strongly on the hydrophobic polymer layers. This is consistent with data collected from unstructured samples of either gold or silicon substrates coated with spacer layers with variable thickness (Figure 3h,i), as the coatings in Figure 3c,g both fall into the thickness range where the fluorescent molecules on the polymer-coated gold have lower intensity than the polymer-coated silicon.

Although both, gold and silicon substrates, give rise to the characteristic features of fluorescence interference contrast, gold substrates give a larger enhancement of the fluorescence signal than silicon substrates measured relative to a transparent glass substrate (which does not cause interference contrast). The enhancement seems to depend on different fluorophores and the excitation wavelengths (Figure 1 and 3, see also Note 3 in the Supporting Information) and can be as high as 18 times higher for surface immobilized Alexa Fluor 555 hydrazide on the CVD polymer coated gold surface. The interference pattern above the gold substrate is shifted 20 nm toward lower spacer thicknesses relative to the silicon substrate, a phenomenon, which has not been previously described and likely arises from differences in the reflective properties between metal and polished silicon surfaces. The experimental data are consistent with our theoretical predictions as shown in Figure 1c and Figure 3h,i. The fitting procedure is described in Note 4 in the Supporting Information.

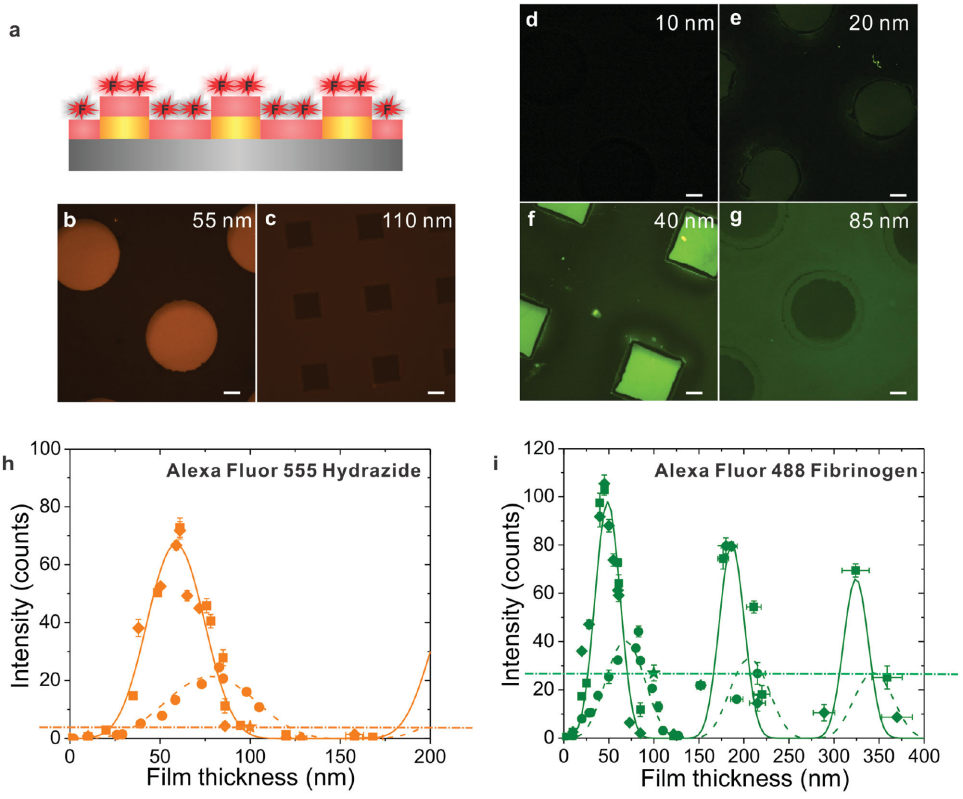

Figure 3. Comparison of surface-modulated fluorescence interference contrast on CVD-coated gold and silicon substrates. a) Nanoscale films of polymer 1 with thicknesses of 55 and 110 nm were homogeneously deposited on a silicon wafer featuring gold islands. b,c) Fluorescence microscopy images of Alexa Fluor 555 hydrazide dye immobilized on these substrates. d–g) Fluorescence microscopy images of Alexa Fluor 488 fibrinogen immobilized on the gold patterned silicon surface coated with CVD polymer 1 films with thicknesses of 10nm, 20, 40, and 85 nm, respectively. h,i) The relationship of the fluorescence intensity versus the polymer spacer layer thickness for immobilized Alexa Fluor 555 hydrazide or Alexa Fluor 488 fibrinogen. The polymer spacer layers were deposited on gold with a thickness of 35 nm (squares) and 100 nm (diamonds), silicon (circles) and glass (star/dash-dot line). No difference in fluorescence intensity was observed for samples with 35 or 100 nm gold layers. Scale bars represent 100 µm.

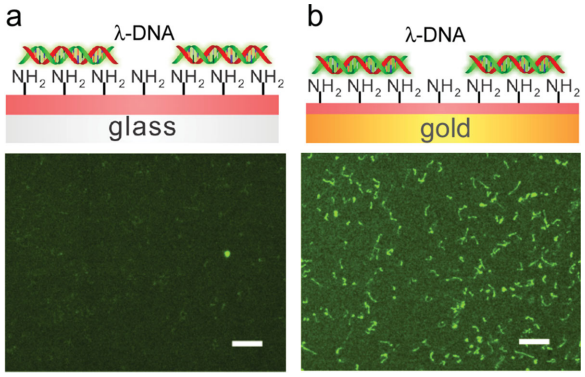

Figure 4. Imaging of single DNA molecules using nanoscale amplification substrates. Lambda DNA stained with SYBR gold was adsorbed on films of polymer 2 (with amine group) coated at different thicknesses on different substrates. a) 100 nm polymer 2 coated on a glass surface. b) 55 nm polymer 2 coated on a gold surface. All samples were incubated in the DNA solution (50 ng mL^{-1}) for 30 min followed by thorough rinsing and air blow drying. Scale bars represent 10 μm.

The potential of nanoscale fluorescence amplification substrates for biomacromolecule studies is illustrated by imaging lambda-DNA stained with SYBR Gold (**Figure 4**). Lambda-DNA is a large double-strand DNA molecule with 2 nm diameter and 16 μm contour length.[34] The fluorophore SYBR Gold has a good quantum yield of ≈0.6.[35] Here we selected the amino-functionalized polymer 2 coating as the nanoscale amplification layer. For comparison, amino-functionalized organosilanes such as 3-aminopropyl-triethoxysilanes (APTES) are commonly used to treat mica and glass surfaces to immobilize and condense DNA molecules.[36] Similar to APTES-treated glass, amino-functionalized polymer 2 interacts with DNA in water via the electrostatic interactions between positively charged amino groups and negatively charged phosphate groups on the DNA backbone.[34] However, in contrast to APTES, polymer 2 can be deposited as films with precisely controllable thickness. While adsorbed DNA molecules display low levels of emitted fluorescence on bare glass or glass coated with polymer 2 (Figure 4a), the gold substrate coated with polymer 2 at an optimum layer thickness of 55 nm enables clear observation of single DNA molecules at the same microscope and camera settings. We attribute the threefold fluorescence enhancement to the particular setup of the fluorescence amplification substrate.

Fluorescence amplifying substrates and lock-in analysis can be integrated into established biosensor concepts, such as immunofluorescence assays.[37] In **Figure 5**, biotin–PEG–hydrazide was immobilized onto the aldehyde-functionalized

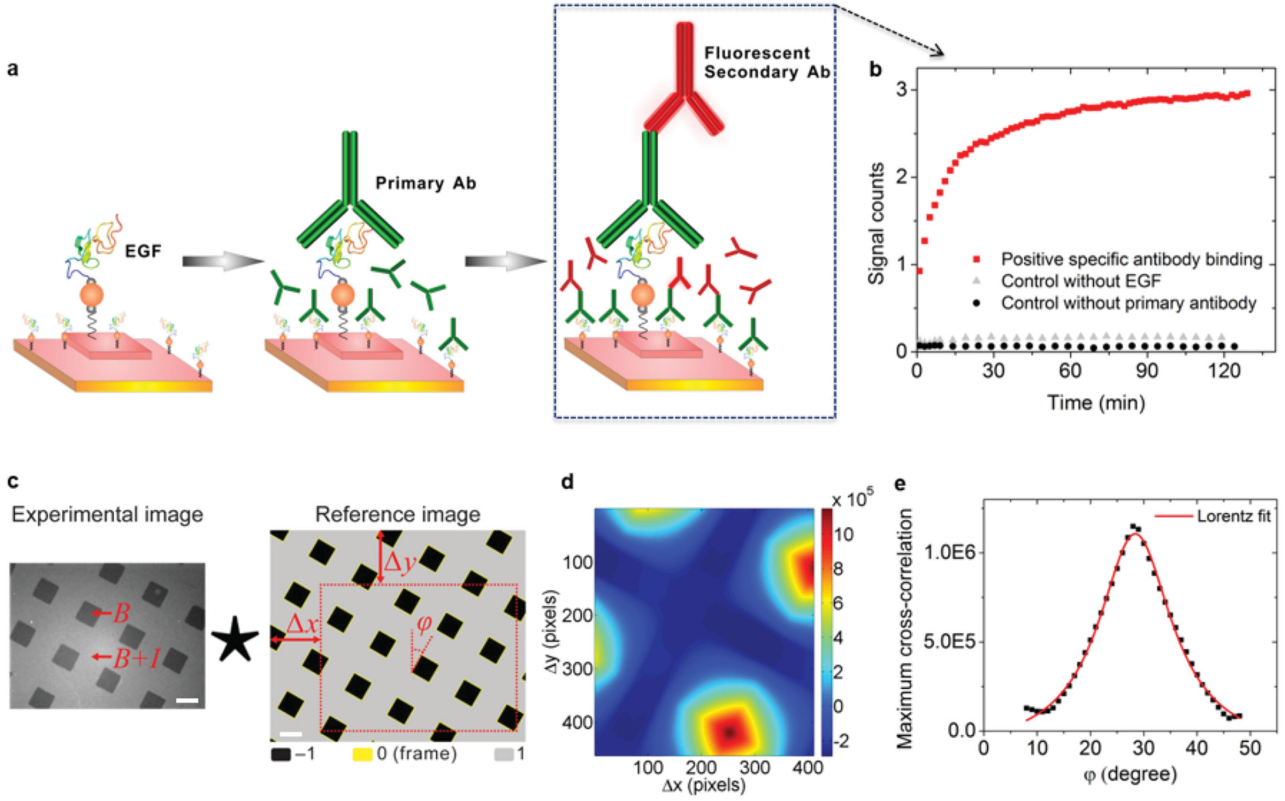

Figure 5. Real-time monitoring of immunofluorescence antibody binding via lock-in analysis. a) Immobilization of EGF, a primary antibody against EGF and a secondary antibody conjugated with the Alexa 647 fluorescent dye. b) The red solid squares present the binding kinetics of the secondary antibody (20 μg mL^{-1}) to the surface-bound primary antibody in goat serum. The gray solid triangles show the results obtained on a control experiment that lacked the EGF, but otherwise was treated identically. The black solid squares show the results of a second control experiment that lacked the primary antibody immobilization step, but was otherwise treated identically. All data shown in this graph were generated by lock-in analysis from the fluorescence microscopy images taken every 60 s. A typical example of the lock-in image analysis is presented. c) Lock-in analysis scheme. Scale bars represent 200 μm. d) Cross-correlation at a selected angle $\varphi = 28°$. e) Maximum cross-correlation at different φ.

CVD coating (polymer **1**). In a second step, the biotinylated surface was allowed to react with streptavidin. Finally, epidermal growth factor (EGF) labeled with a biotin conjugate was attached to this modified surface. To detect EGF, a primary antibody against EGF was incubated with the substrate and the binding of fluorescence-labeled secondary antibody in goat serum was monitored in real time (Figure 5b). A difference in the fluorescence signal between test and reference regions was not observed, when either the EGF or the primary antibody were omitted in the assay, indicating specific binding. More details of this experiment are shown in Note 5 in the Supporting Information. Again, the ultrasensitive detection of miniscule increases in the fluorescence signal of the test regions is enabled by lock-in analysis algorithms, whose key steps are detailed in Figure 5c–e.

In summary, we have demonstrated that nanoscale polymer films deposited on gold surfaces can be used for real-time monitoring of protein adsorption, single molecule behavior, and antibody binding. CVD polymerization of the spacer layers provides thickness control with nanometer accuracy, facile micro/nanofabrication integration and simultaneous functionalization and deposition within one single step. The functional groups presented by the spacer layer can be selected within a wide range according to specific needs of the biomedical applications. The application of lock-in analysis algorithms enables detection of minute changes in the fluorescence signal on the patterned surface; even in the presence of a high background such as goat serum. The herein described substrates and fluorescence analysis methodology are applicable to a wide selection of fluorescent molecules with different excitation/emission wavelengths and can be integrated into a variety of detection platforms. The low-cost fabrication of the patterns and the absence of additional requirements for the fluorescence imaging setups imply that patterned reactive polymer layers with nanometer thickness on gold substrates can be widely used for fluorescence-based biosensors.

Experimental Section

Gold Coating: Polished 4 in. silicon wafers (Silicon Valley Microelectronics, Inc.) were coated by a Denton Vacuum DV-502A E-Beam Evaporator according to the standard operation procedure. First, a 5 nm Ti adhesion layer and then 35 or 100 nm gold was coated at 1.0 Å s^{-1}. Metal patterns were generated by applying poly(dimethylsiloxane) (PDMS) microstencils on the wafers before loading them into the E-beam evaporator. The microstencils were well adhered to the wafers during the coating process. The details for the microstencils preparation were reported in our previous papers.[38,39]

CVD Polymerization and Characterization: Poly(4-chloro-*p*-xylylene), poly(formyl-*p*-xylylene) (polymer **1**) and poly[(4-aminomethyl-*p*-xylylene)-*co*-(*p*-xylylene)] (polymer **2**) were synthesized via CVD polymerization. Details about the deposition of these polymers have been reported before except polymer **1** (Preparation and characterization of the new polymer 1 are shown in Note 6 in the Supporting Information). To generate surfaces with polymer micropatterns by multiple-step CVD as shown in Figure 1 and 2, the polymer was coated on the surface multiple times with different precursor feed amount and with the help of PDMS microstencils. FTIR spectra of the CVD polymer films were recorded on a Nicolet 6700 spectrometer with the grazing angle accessory (Smart SAGA) with a 80° fixed angle of incidence. XPS spectra were acquired on an Axis Ultra X-ray photoelectron spectrometer (Kratos Analyticals, UK) equipped with a monochromatized Al Kα X-ray source. Thicknesses of patterned coatings were measured on silicon or gold substrates with an Imaging Spectroscopic Ellipsometer (Accurion, Nanofilm EP^3-SE) with 1 µm lateral resolution. Ellipsometric parameters were fitted using the Cauchy model.

Fluorescence *Imaging*: Real-time monitoring of protein adsorption or antibody binding were carried out with an epifluorescence microscope (Nikon Eclipse 80i) with a standard setup as shown in Figure 1. A FluorChem M (ProteinSimple, USA) digital dark room was used for imaging a series of fluorescent molecule immobilized surfaces with different polymer spacer layer thicknesses.

Image Analysis: A reference image U_{ref} was created with the pattern used in the CVD process to structure the surface, but with 1.5-fold larger linear dimensions compared to the camera image U_{in}. The intensity values of the reference image were set to +1 in test areas, –1 in reference areas, and 0 in 6-pixel wide stripe on the border between the reference areas and the test areas. The reference image was cross-correlated with the camera image U_{in}, for all possible rotation angles in 1° steps and all possible lateral offsets in 1 pixel steps. At a given rotation angle, the resulting cross-correlation values will show multiple local maxima due to the periodicity of the pattern (Figure 5d). The global maximum at a given angle in turn is maximized when the reference image and the camera image are perfectly rotationally aligned (Figure 5e). The maximum cross-correlation value $(U_{in} * U_{ref})_{max}$ and optimal rotation are determined by fitting with a Lorentz function and are related to the signal intensity I, the background intensity B, the number of total pixels in the experimental image N_{pixel} and the image noise ε by a system of two equations:

$$\frac{1}{2} I N_{pixel} + B \sum_{all\ pixel} U_{ref} = (U_{in} * U_{ref})_{max} \quad (1)$$

$$\frac{1}{2} I \sum_{all\ pixel} U_{ref} + B N_{pixel} + \sum_{all\ pixel} \varepsilon = \mathcal{F}(0,0) \quad (2)$$

Equation (2) represents the base component of the Fourier transform of the experimental image $\mathcal{F}(0,0)$. The intensity values I and B are obtained by solving the system of Equation (1) and (2) under the assumption that – for a large image – the image noise E has the property:

$$\frac{\sum_{all\ pixels} \varepsilon}{N_{pixel}} \to 0 \quad (3)$$

A detailed analysis of the algorithm and its performance as a function of noise levels and pattern parameters is forthcoming.

Supporting Information

Supporting Information is available online from the Wiley Online Library or from the author.

Acknowledgements

X.D. and S.H. contributed equally to this work. This work was supported by the Defense Threat Reduction Agency under award numbers HDTRA 1-12-1-0037 and HDTRA 1-12-1-0039. S.H. and F.X. acknowledge partial support by the Chinese Scholarship Council. In addition, the authors acknowledge the valuable and insightful discussions with Brian Pate.

Received: October 21, 2015
Revised: November 20, 2015
Published online: January 25, 2016

[1] S. W. Hell, *Science* **2007**, *316*, 1153.
[2] N. Panchuk-Voloshina, R. P. Haugland, J. Bishop-Stewart, M. K. Bhalgat, P. J. Millard, F. Mao, W. Y. Leung, R. P. Haugland, *J. Histochem. Cytochem.* **1999**, *47*, 1179.

[3] R. S. Tuma, M. P. Beaudet, X. K. Jin, L. J. Jones, C. Y. Cheung, S. Yue, V. L. Singer, *Anal. Biochem.* **1999**, *268*, 278.
[4] K. Skonieczny, A. I. Ciuciu, E. M. Nichols, V. Hugues, M. Blanchard-Desce, L. Flamigni, D. T. Gryko, *J. Mater. Chem.* **2012**, *22*, 20649.
[5] X. Michalet, F. F. Pinaud, L. A. Bentolila, J. M. Tsay, S. Doose, J. J. Li, G. Sundaresan, A. M. Wu, S. S. Gambhir, S. Weiss, *Science* **2005**, *307*, 538.
[6] X. Y. Wang, X. F. Ren, K. Kahen, M. A. Hahn, M. Rajeswaran, S. Maccagnano-Zacher, J. Silcox, G. E. Cragg, A. L. Efros, T. D. Krauss, *Nature* **2009**, *459*, 686.
[7] K. Rurack, M. Spieles, *Anal. Chem.* **2011**, *83*, 1232.
[8] K. Aslan, I. Gryczynski, J. Malicka, E. Matveeva, J. R. Lakowicz, C. D. Geddes, *Curr. Opin. Biotechnol.* **2005**, *16*, 55.
[9] J. R. Lakowicz, *Anal. Biochem.* **2005**, *337*, 171.
[10] C. D. Geddes, J. R. Lakowicz, *J. Fluoresc.* **2002**, *12*, 121.
[11] J. R. Lakowicz, *Anal. Biochem.* **2001**, *298*, 1.
[12] N. Ganesh, W. Zhang, P. C. Mathias, E. Chow, J. Soares, V. Malyarchuk, A. D. Smith, B. T. Cunningham, *Nat. Nanotechnol.* **2007**, *2*, 515.
[13] J. C. Waters, *J. Cell Biol.* **2009**, *185*, 1135.
[14] S. W. Hell, E. H. K. Stelzer, *Handbook of Biological Confocal Microscopy*, (Ed: J. B. Pawley), Plenum Press, New York, **1995**.
[15] D. E. Wolf, C. Samarasekera, J. R. Swedlow, in *Quantitative Analysis of Digital Microscope Images*, Vol. *81*, (Eds: G. Sluder, D. E. Wolf), Elsevier Academic Press, San Diego, CA, USA, **2007**.
[16] A. Hucknall, D.-H. Kim, S. Rangarajan, R. T. Hill, W. M. Reichert, A. Chilkoti, *Adv. Mater.* **2009**, *21*, 1968.
[17] M. Cretich, M. R. Monroe, A. Reddington, X. Zhang, G. G. Daaboul, F. Damin, L. Sola, M. S. Unlu, M. Chiari, *Proteomics* **2012**, *12*, 2963.
[18] J. H. Scofield, *Am. J. Phys.* **1994**, *62*, 129.
[19] A. Lambacher, P. Fromherz, *Appl. Phys. A: Mater.* **1996**, *63*, 207.
[20] J. Kerssemakers, J. Howard, H. Hess, S. Diez, *Proc. Natl. Acad. Sci. USA* **2006**, *103*, 15812.
[21] J. W. J. Kerssemakers, T. R. Blosser, C. Dekker, *Nano Lett.* **2014**, *14*, 4469.
[22] A. Lambacher, P. Fromherz, *J. Opt. Soc. Am. B* **2002**, *19*, 1435.
[23] E. Fort, S. Gresillon, *J. Phys. D: Appl. Phys.* **2008**, *41*, 013001.
[24] A. Renier, T. Mangeat, H. Benalia, C. Elie-Caille, C. Pieralli, B. Wacogne, *Laser Phys.* **2010**, *20*, 591.
[25] K. Lee, L. D. Hahn, W. W. Yuen, H. Vlamakis, R. Kolter, D. J. Mooney, *Adv. Mater.* **2011**, *23*, H101.
[26] J. Zhang, J. R. Lakowicz, *Opt. Express* **2007**, *15*, 2598.
[27] P. J. Tarcha, J. DeSaja-Gonzalez, S. Rodriguez-Llorente, R. Aroca, *Appl. Spectrosc.* **1999**, *53*, 43.
[28] J. B. Fortin, *Chemical Vapor Deposition Polymerization: The Growth and Properties of Parylene Thin Films*, Kluwer Academic Publishers, Boston, MA, USA, **2004**.
[29] F. Bally, K. Cheng, H. Nandivada, X. P. Deng, A. M. Ross, A. Panades, J. Lahann, *ACS Appl. Mater. Inter.* **2013**, *5*, 9262.
[30] H. Hess, D. S. Larsen, A. A. Scheidemann, *Philos. Mag. B*, **1999**, *79*, 1437.
[31] A. Scheidemann, H. Hess (University of Washington), *US Patent 1573770*, **2008**.
[32] D. M. Dobkin, *Principles of Chemical Vapor Deposition*, Kluwer Academic Publishers, Dordrecht, The Netherlands, **2003**.
[33] X. P. Deng, J. Lahann, *J. Appl. Polym. Sci.* **2014**, *131*, 40315.
[34] H. G. Hansma, I. Revenko, K. Kim, D. E. Laney, *Nucleic Acids Res.* **1996**, *24*, 713.
[35] I. Johnson, M. T. Z. Spence, *The Molecular Probes Handbook: A Guide to Fluorescent Probes and Labeling Technologies*, Life Technologies Corporation, Carlsbad, CA, USA, **2010**.
[36] Y. Lyubchenko, L. Shlyakhtenko, R. Harrington, P. Oden, S. Lindsay, *Proc. Natl. Acad. Sci. USA* **1993**, *90*, 2137.
[37] J.-l. Ru, Y. Zhao, X.-x. Xie, G.-z. Che, C.-f. Cheng, H.-m. Zhao, Z.-y. Jin, H.-p. Sun, X.-f. Li, *Pediatr. Res.* **2015**, *77*, 376.
[38] X. W. Jiang, H. Y. Chen, G. Galvan, M. Yoshida, J. Lahann, *Adv. Funct. Mater.* **2008**, *18*, 27.
[39] H. Y. Chen, J. Lahann, *Adv. Mater.* **2007**, *19*, 3801.